


Electrical Control of Valley-Zeeman Spin-Orbit-Coupling-Induced Spin Precession at Room Temperature

Josep Inгла-Aynés^{1,*}, Franz Herling¹, Jaroslav Fabian², Luis E. Hueso^{1,3}, and Fèlix Casanova^{1,3,†}

¹*CIC nanoGUNE BRTA, 20018 Donostia-San Sebastian, Basque Country, Spain*

²*Institute for Theoretical Physics, University of Regensburg, 93040 Regensburg, Germany*

³*IKERBASQUE, Basque Foundation for Science, 48013 Bilbao, Basque Country, Spain*

 (Received 13 November 2020; revised 19 February 2021; accepted 11 June 2021; published 21 July 2021)

The ultimate goal of spintronics is achieving electrically controlled coherent manipulation of the electron spin at room temperature to enable devices such as spin field-effect transistors. With conventional materials, coherent spin precession has been observed in the ballistic regime and at low temperatures only. However, the strong spin anisotropy and the valley character of the electronic states in 2D materials provide unique control knobs to manipulate spin precession. Here, by manipulating the anisotropic spin-orbit coupling in bilayer graphene by the proximity effect to WSe₂, we achieve coherent spin precession in the absence of an external magnetic field, even in the diffusive regime. Remarkably, the sign of the precessing spin polarization can be tuned by a back gate voltage and by a drift current. Our realization of a spin field-effect transistor at room temperature is a cornerstone for the implementation of energy efficient spin-based logic.

DOI: [10.1103/PhysRevLett.127.047202](https://doi.org/10.1103/PhysRevLett.127.047202)

The realization of logic operations using the spin degree of freedom is a crucial goal for spintronics [1–5]. In this context, one of the most studied theoretical proposals is that of Datta and Das [6], which requires spin precession around the spin-orbit fields (SOFs) and has raised considerable interest [5–9]. However, the experimental achievement of the required strong spin-orbit coupling (SOC) regime in conventional materials can only be realized in ballistic systems with long momentum scattering time (τ_p) and very clean interfaces [7–9]. Consequently, its implementation in all-electrical devices is currently limited to low temperatures [10–15].

Alternatively, graphene-based van der Waals heterostructures are an ideal platform for spin manipulation [16,17] since, in these systems, graphene's low SOC can be enhanced by proximity with transition metal dichalcogenides (TMDs) [18–36]. Such graphene-TMD heterostructures possess a unique spin texture. In particular, the in-plane SOFs are of the Rashba type and point perpendicular to the electronic momentum. In the weak SOC regime, Rashba SOC caused by the stack inversion asymmetry leads to out-of-plane spin relaxation rates of $(\tau_s^\perp)^{-1} = \Omega_R^2 \tau_p$, where Ω_R is the Larmor frequency around the Rashba SOFs. In contrast, the out-of-plane SOFs, which arise due to the broken sublattice symmetry in the TMD being imprinted on graphene, have opposite sign at the K and K' valleys [see Fig. 1(a)] to preserve time reversal symmetry [18]. These SOFs, commonly called valley-Zeeman SOFs, give rise to spin-valley locking. In this case, the intervalley scattering time (τ_{iv}) is the characteristic timescale dominating the spin dynamics. Hence, in the

weak SOC regime, the in-plane spin relaxation rate is given by $(\tau_s^\parallel)^{-1} = \Omega_{VZ}^2 \tau_{iv} + (2\tau_s^\perp)^{-1}$, where Ω_{VZ} is the Larmor frequency around the valley-Zeeman SOFs. Since τ_{iv} is typically much longer than τ_p [37], $\tau_{iv}\Omega_{VZ}$ becomes significantly bigger than $\tau_p\Omega_R$ and, as a consequence, the spin transport is highly anisotropic [23–27]. Unlike in conventional materials, the spin-valley locking present in graphene-TMD heterostructures might enable the strong SOC regime if τ_{VZ} would become comparable to τ_{iv} , where $\tau_{VZ} = 2\pi/\Omega_{VZ}$ is the in-plane spin precession period around the out-of-plane valley-Zeeman SOFs [Fig. 1(b)]. Such a condition may even be achieved in the diffusive regime and could allow for room temperature operations.

In this Letter, we report the achievement of the strong SOC regime in bilayer graphene (BLG)-WSe₂ heterostructures, leading to magnetic-field free spin precession induced by the valley-Zeeman SOC as shown in Figs. 1(a) and 1(b). Furthermore, by tuning the carrier density using a back-gate voltage (V_{bg}) and the spin transport time using a drift current (I_{DC}), we control the spin polarization up to room temperature, making our device operate as a Datta-Das spin field-effect transistor [see Figs. 1(c) and 1(d)]. This hitherto unreported performance paves the way for the achievement of highly functional logic circuits [5,38].

To measure SOC-induced spin precession, we prepared 2- μm -wide [the heterostructure width is defined as W_{TMD} in Fig. 2(a)] BLG-WSe₂ lateral spin valves with spin-polarized TiO_x/Co contacts and Ti/Au reference electrodes [Fig. 2(a)]. BLG was chosen to take advantage of its gate tunable diffusivity. To ensure an efficient SOC and achieve the strong SOC regime, we chose WSe₂, the TMD that

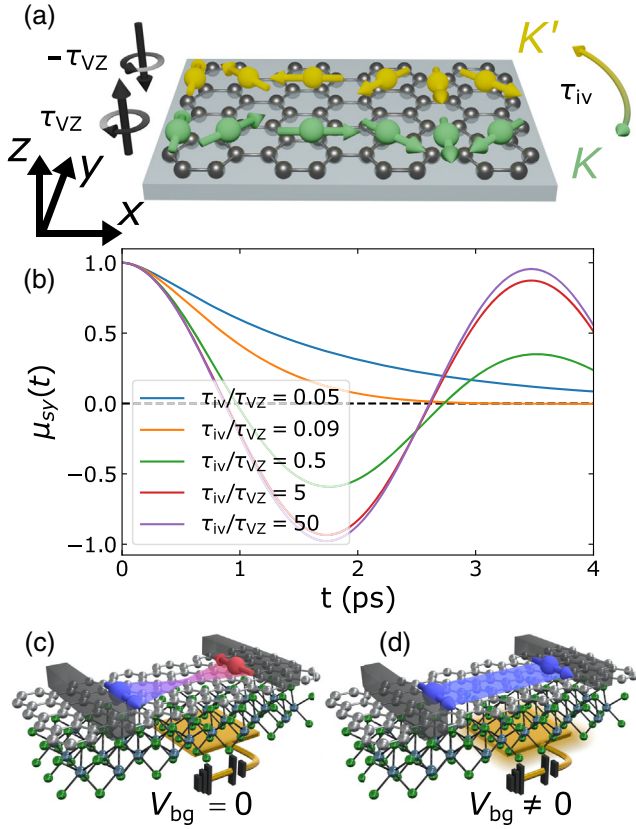


FIG. 1. Device working principle and BLG-WSe₂ spin transistor operation. (a) Sketch of a BLG-WSe₂ heterostructure. Out-of-plane valley-Zeeman SOF (black arrows) with opposite sign at the K and K' valleys induce in-plane spin precession with a period τ_{VZ} . Spins can scatter between the valleys via intervalley scattering (τ_{IV}). (b) Time dependence of the spin accumulation μ_{sy} for different τ_{IV} values (see Ref. [39] for details). μ_{sy} undergoes net precession for $\tau_{IV} \geq 0.5\tau_{VZ}$. (c) and (d) Sketch of a spin field-effect transistor operating at the strong SOC regime where the valley-Zeeman induced spin precession is tuned by V_{bg} to control the sign reversal.

imprints the largest valley-Zeeman SOC on graphene [18], and annealed the van der Waals heterostructures at 430 °C. See Ref. [39] for the fabrication details, reproducibility, the role of the annealing temperature, and the role of W_{TMD} on the measured signals.

The diffusive spin transport experiments are performed in the nonlocal geometry [circuit in Fig. 2(a), see Ref. [39] for measurement details]. The y -spin accumulation (μ_{sy}) induced by applying a current $I_{\delta 1}$ through contact 3 diffuses across the channel and builds a voltage difference $V_{\delta 1} = P_d \mu_{sy} / e$ between contacts 4 and 7. Here, P_d is the detector spin polarization and e the electron charge. The nonlocal resistance ($R_{nl} = V_{\delta 1} / I_{\delta 1}$) is measured as a function of a magnetic field applied along y (B_y) in the conventional spin valve experiment. Figure 2(b) shows that, for $V_{bg} = 50$ V, R_{nl} in the antiparallel magnetization state (R_{nl}^{AP}) is higher than in the parallel one (R_{nl}^P). The spin

signal, which is defined as $\Delta R_{nl} = (R_{nl}^P - R_{nl}^{AP})/2$, is thus negative. This observation could be a consequence of the sought in-plane spin precession induced by the valley-Zeeman coupling, although it could also be caused by the spin injector and detector having opposite spin polarizations [56,57].

To confirm that μ_{sy} is reversed during transport as in Fig. 1(b), we induce out-of-plane spin precession by measuring R_{nl} as a function of a magnetic field applied along x (B_x) [see Fig. 2(c)]. In the parallel configuration, R_{nl}^P has a local maximum at $B_x = 0$, when the spins are not precessing. Then, R_{nl}^P decreases until it reaches a minimum *shoulder* ($B_x \approx \pm 0.1$ T) when the average precession angle at the detector is of 180°. In this case, the spins injected along y cross the TMD-covered region pointing along z , and reach the detector pointing along $-y$. At higher B_x , R_{nl}^P increases until it merges with R_{nl}^{AP} and ΔR_{nl} reaches zero as the spins dephase and the contact magnetizations are pulled toward x . In contrast, R_{nl}^{AP} shows a minimum at $B_x = 0$, where it is higher than R_{nl}^P . As B_x increases, R_{nl}^{AP} also increases leading to an enhancement of ΔR_{nl} with B_x [Fig. 2(c), inset]. This result is in stark contrast with standard spin precession measurements (where ΔR_{nl} decreases at low B , until it reverses sign when the precessed angle is of 90° [24,25]) and is a direct consequence of μ_{sy} being reversed with respect to the out-of-plane spin accumulation. Finally, R_{nl}^{AP} reaches a maximum when the precessed angle at the detector is of 180°, before the contact magnetization pulling and spin dephasing decrease the spin signal until it vanishes for $B_x > 0.2$ T. We observe that (i) the magnitude of the in-plane spin signal ($B_x = 0$) is significantly smaller than the out-of-plane one ($B_x \approx \pm 0.1$ T), in agreement with previous works in graphene-TMD heterostructures [23–27]; (ii) in contrast to the in-plane signal, the out-of-plane one is not reversed. This observation, together with the fact that out-of-plane spins are in the weak SOC regime [39], indicates that the sign reversal is not caused by the opposite sign of the injector and detector spin polarizations. Hence, μ_{sy} must be reversed during transport. Spin transport experiments performed at the pristine BLG region show conventional positive signal for all V_{bg} values [39], evidencing that the sign reversal occurs across the TMD-covered region. Since the in-plane spin signal is negative without an applied magnetic field, we conclude that our experiments are probing the strong SOC regime. Note that our result provides the most direct experimental evidence that spin precession occurs between scattering events in graphene-TMD heterostructures [21–27].

In Fig. 2(d) (black curve), we plot the spin signal as a function of V_{bg} . The data show that the signal is negative for $V_{bg} > 20$ V and $V_{bg} < -40$ V. For -40 V $< V_{bg} < 20$ V, ΔR_{nl} is below the noise level (see Ref. [39] for the raw data). To understand the gate dependence, one must take into account the SOC in the

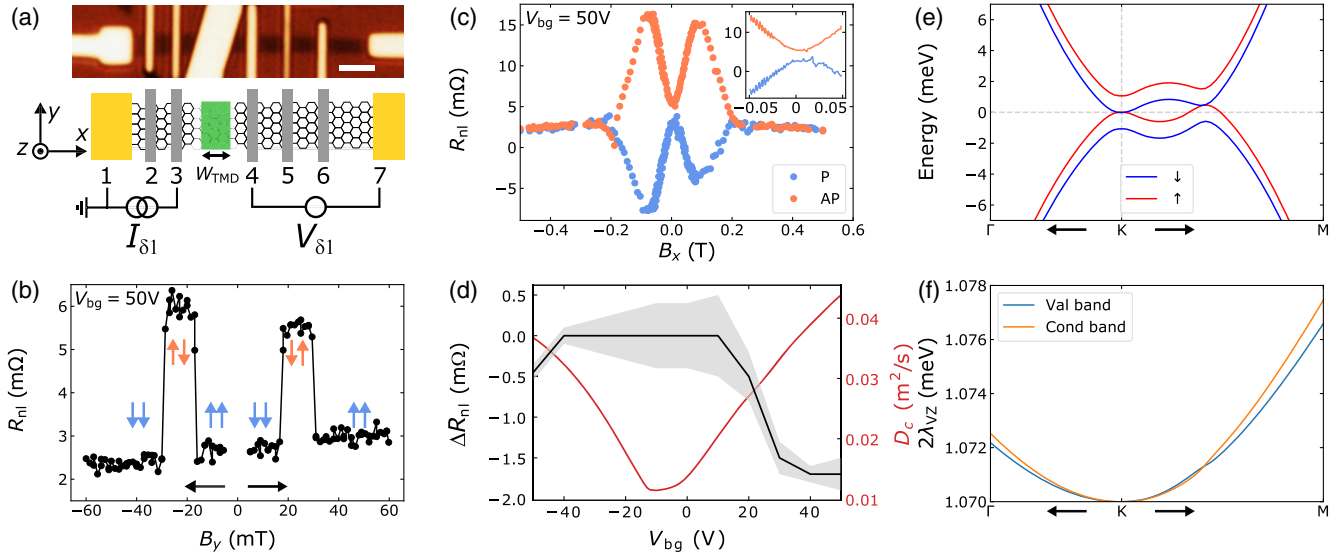


FIG. 2. Diffusive spin transport at 50 K. (a) Optical image of the measured device. The BLG flake is the dark horizontal stripe and WSe₂ is the bright flake in the middle. The scale bar is 2 μm . The bottom panel shows a sketch of the device with the WSe₂-covered BLG region shown in green. The circuit corresponds to the standard nonlocal spin diffusion measurement configuration. Contacts 1 and 7 are not magnetic (Ti/Au) and 2 to 6 are spin-polarized TiO_x/Co contacts. (b) Nonlocal spin valve measurement across the WSe₂-covered BLG region as a function of the magnetic field applied along y (B_y) for $V_{\text{bg}} = 50$ V. The horizontal arrows represent the B_y -sweep direction and the vertical ones the magnetization of contacts 3 and 4. (c) Nonlocal spin precession measurements with the magnetic field applied along x (B_x) in the parallel (P) and antiparallel (AP) configurations for $V_{\text{bg}} = 50$ V. Inset: low field detail. (d) Spin signal (ΔR_{nl}) and charge diffusivity (D_c) as a function of V_{bg} . (e) Spin-polarized band structure of BLG-WSe₂ at zero electric field. The red lines represent spin-up (along $+z$) and the blue ones spin-down (along $-z$). (f) Spin splitting ($2\lambda_{\text{VZ}}$) of the valence and conduction bands obtained from the band structure in panel e.

BLG-WSe₂ heterostructure. As reported recently [28–30], the SOC in BLG-TMD heterostructures can have a pronounced electric field dependence. To obtain the V_{bg} dependence of the SOC in our system, we have used the tight-binding Hamiltonian shown in Ref. [30] (see also Ref. [39]). To explain the symmetric dependence of ΔR_{nl} vs V_{bg} with respect to the charge neutrality point, we have assumed that both layers have the same potential, which means that the externally applied field compensates for the internal 0.267 V/nm induced by the WSe₂ on the BLG at the charge neutrality point [28]. The results from this band-structure calculation are displayed in Figs. 2(e) and 2(f) and show perfect agreement with Ref. [28]. As expected, the conduction and valence bands cross at the K point because of the layer-symmetric configuration. Looking at the spin splitting ($2\lambda_{\text{VZ}} = \hbar\Omega_{\text{VZ}}$, where \hbar is the reduced Plank constant) in Fig. 2(f), we observe that it depends very weakly with the energy, indicating that the proximity SOC remains almost constant through the calculated energy range. This observation implies that the V_{bg} dependence of the SOC is unlikely to be the reason for the observed gate dependence. As shown in Fig. 1(b) and Ref. [39], if τ_{iv} changes with V_{bg} [37], it can tune the spin precession frequency but, since proximitized graphene shows weak antilocalization [19–22], we could not measure weak localization in our device to extract τ_{iv} . In contrast, the charge diffusivity (D_c) of the BLG decreases significantly

near the charge neutrality point [see red curve in Fig. 2(d) and Ref. [39]]. As shown by our spin transport calculations [39], changes in D_s (which we obtain assuming $D_s = D_c$ [58]), can have a crucial influence on the spin signal in the strong SOC regime, making D_s the most likely responsible for the measured V_{bg} dependence. However, the electron-hole asymmetry in ΔR_{nl} indicates that other factors such as spin absorption by the WSe₂ [59,60] may also play a role. Note that we cannot discard a sign change of the signal below the noise level near the charge neutrality point.

By tuning the spin dynamics in the strong SOC regime, it should be possible to control the ΔR_{nl} sign in a magnetic-field free device geometry. To confirm our hypothesis, we perform spin transport experiments under the effect of carrier drift in the geometry shown in Fig. 3(a). The carrier drift is induced by I_{DC} , which is applied between contacts 4 and 1, and the spin current injected at contact 3 is detected as a nonlocal signal ($R_{\text{nl}} = V_{\delta 2}/I_{\delta 2}$) between contacts 5 and 7. Since $V_{\delta 2}$ is coupled to $I_{\delta 2}$, our measurement excludes the DC spin current injected by contact 4 [39]. The applied I_{DC} induces a drift velocity $v_d = I_{\text{DC}}/(W_{\text{BLG}}ne)$, where n is the carrier density in the channel and W_{BLG} is the BLG flake width. The induced v_d changes the spin transport time across the BLG-WSe₂ [61–63], leading to a tuning of the spatial oscillation frequency of μ_{sy} [39]. In Fig. 3(b), we present spin valve

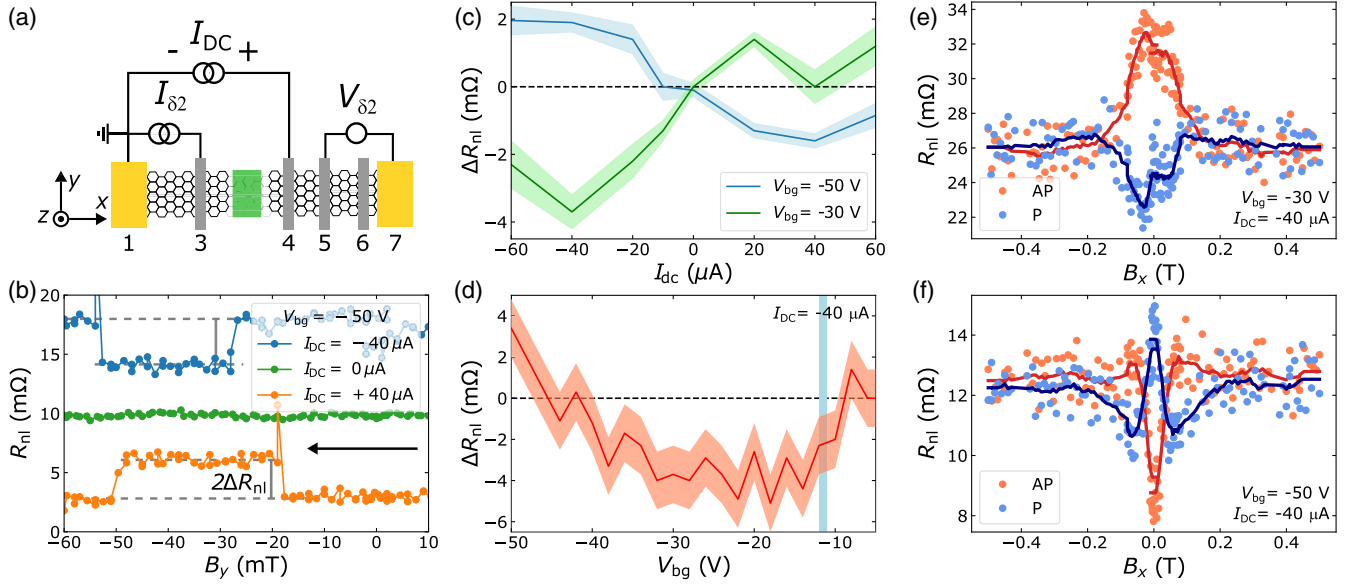


FIG. 3. Controlling spin transport with drift at 50 K. (a) Sketch of the device with the spin drift measurement configuration. (b) Nonlocal spin valve measurements for $V_{bg} = -50$ V at $I_{DC} = -40, 0$, and $+40$ μA . The curves have been shifted for clarity. (c) I_{DC} dependence of ΔR_{nl} at $V_{bg} = -50$ and -30 V. (d) ΔR_{nl} vs V_{bg} at $I_{DC} = -40$ μA . The vertical light blue line is the charge neutrality point of the WSe₂-covered BLG region. (e),(f) Nonlocal spin precession measurements with B_x in the P and AP configurations for $I_{DC} = -40$ μA and $V_{bg} = -30$ V and -50 V, respectively. The lines are obtained by averaging over a window of eleven points.

measurements at $V_{bg} = -50$ V and $I_{DC} = -40, 0$, and 40 μA . We observe that, in contrast with the results obtained from spin drift experiments in the pristine graphene region [39], ΔR_{nl} reverses sign as we sweep I_{DC} from -40 to 40 μA , and becomes smaller than the noise level for $I_{DC} = 0$. This result is the first demonstration of carrier drift control of spin reversal in an all-electrical device. Such unprecedented observation is consistent with the spin transport model shown in Figs. 1(a) and 1(b) if the in-plane spin precession angle at $I_{DC} = 0$ is an odd multiple of 90° (see Ref. [39] for more detailed calculations). A comprehensive illustration of this behavior is shown in Fig. 3(c), where we plot ΔR_{nl} vs I_{DC} as extracted from spin valve measurements performed at $V_{bg} = -50$ and -30 V (see Ref. [39] for the complete set of data). Importantly, we find that ΔR_{nl} reverses sign between the two V_{bg} for all the I_{DC} values. To explain this sign reversal, we consider λ_{VZ} , τ_{iv} , and D_s , that are the relevant parameters that could change with V_{bg} (note that τ_s^\perp and n , that changes v_d , cannot explain the observed sign reversal, see Ref. [39] for details). We dismiss λ_{VZ} because, according to our tight-binding calculations [Figs. 2(e) and 2(f)], the valley-Zeeman SOC does not have a significant dependence with V_{bg} . As mentioned above, τ_{iv} may change with V_{bg} [37] and modify the effective spin precession frequency, as shown in Fig. 1(b) and [39]. Finally, we consider the change in D_s from 0.01 to 0.03 m^2/s and observe that it has a strong influence on the μ_{sy} spatial frequency [39]. Even though both τ_{iv} and D_s could be responsible for the sign

reversal of ΔR_{nl} with V_{bg} , the extracted change in D_s is large enough to explain a sign reversal keeping τ_{iv} constant.

Our observation of a sign reversal in ΔR_{nl} with V_{bg} at fixed I_{DC} is very promising for Datta-Das spin field-effect transistor operations which work in the diffusive regime, as sketched in Figs. 1(c) and 1(d). In Fig. 3(d), we plot ΔR_{nl} vs V_{bg} at $I_{DC} = -40$ μA . We find that ΔR_{nl} becomes positive for $V_{bg} < -45$ V and at $V_{bg} = -8$ V.

Finally, we measure spin precession around B_x to confirm that the out-of-plane spin signal has not changed sign and the previous results are indeed caused by in-plane spin precession. The results are shown in Figs. 3(e) and 3(f) for $V_{bg} = -30$ and -50 V, respectively. For $V_{bg} = -30$ V, the spin precession data look similar to that in Fig. 2(c) with the difference that the in-plane $B_x = 0$ signal in Fig. 3(e) is comparable to the maximum signal at the shoulders. As a consequence, the shoulders are less clear than in Fig. 2(c). In contrast, the R_{nl} vs B_x data at $V_{bg} = -50$ V show a conventional spin precession shape where the in-plane spin signal is positive and larger than ΔR_{nl} at the shoulders, more similar to isotropic systems [24,25]. See Ref. [39] for the evolution of the spin precession data with I_{DC} .

To confirm that the measured effect is suitable for applications, we perform spin valve experiments at 300 K as a function of V_{bg} (see Ref. [39] for the raw data). The ΔR_{nl} values are plotted in Fig. 4 for $I_{DC} = \pm 40$ μA . These results are very similar to those at 50 K, demonstrating that our device is in the strong

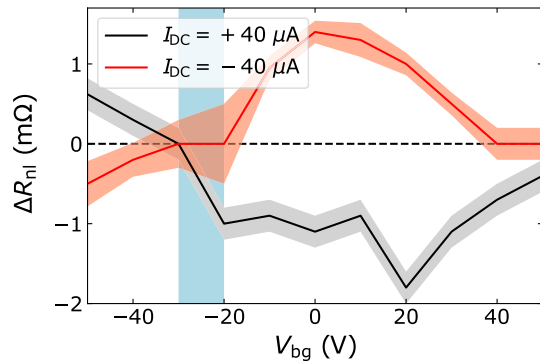


FIG. 4. Room temperature electrical control of spin transport. V_{bg} dependence of ΔR_{nl} for $I_{DC} = \pm 40 \mu A$. The blue area represents the charge neutrality point of the WSe_2 -covered BLG region. ΔR_{nl} reverses sign upon changing the sign of I_{DC} .

SOC regime up to room temperature and the spin orientation can be controlled using both I_{DC} and V_{bg} . Similar results obtained in a second sample are shown in Ref. [39].

To conclude, we demonstrate the valley-Zeeman SOC induced magnetic-field free control of spin precession in a BLG- WSe_2 van der Waals heterostructure at the strong SOC regime. By tuning the carrier density using V_{bg} and the spin transport time using I_{DC} , we control the spin polarization up to room temperature, making our device operate as a spin field-effect transistor. This achievement has prospects for future spin-based logic applications such as nonvolatile and reconfigurable logic [38] and as a complement to the existing spin-logic proposals [1–4].

We acknowledge R. Llopis and R. Gay for technical assistance and C. K. Safeer, N. Ontoso, and K. Zollner for discussions. This work is supported by the Spanish MICINN under the Maria de Maeztu Units of Excellence Programme (MDM-2016-0618) and under Project No. RTI2018-094861-B-100 and by the European Union H2020 under the Marie Skłodowska Curie Actions (0766025-QuESTech). J.F. acknowledges Deutsche Forschungsgemeinschaft (DFG, German Research Foundation) SFB1277 (Project No. 314695032), SPP 2244, and the European Union H2020 under Grant No. 785219. J.I.-A. acknowledges postdoctoral fellowship support from the Juan de la Cierva-Formación program by the Spanish MICINN (Grant No. FJC2018-038688-I).

*j.ingla@nanogune.eu

[†]f.casanova@nanogune.eu

[1] H. Dery, P. Dalal, Ł. Cywiński, and L. J. Sham, Spin-based logic in semiconductors for reconfigurable large-scale circuits, *Nature (London)* **447**, 573 (2007).

- [2] B. Behin-Aein, D. Datta, S. Salahuddin, and S. Datta, Proposal for an all-spin logic device with built-in memory, *Nat. Nanotechnol.* **5**, 266 (2010).
- [3] S. Manipatruni, D. E. Nikonov, C.-C. Lin, T. A. Gosavi, H. Liu, B. Prasad, Y.-L. Huang, E. Bonturim, R. Ramesh, and I. A. Young, Scalable energy-efficient magnetoelectric spin-orbit logic, *Nature (London)* **565**, 35 (2019).
- [4] V. T. Pham, I. Groen, S. Manipatruni, W. Y. Choi, D. E. Nikonov, E. Sagasta, C.-C. Lin, T. A. Gosavi, A. Marty, L. E. Hueso, I. A. Young *et al.*, Spin-orbit magnetic state readout in scaled ferromagnetic/heavy metal nanostructures, *Nature Electronics* **3**, 309 (2020).
- [5] B. Dieny, I. L. Prejbeanu, K. Garello, P. Gambardella, P. Freitas, R. Lehndorff, W. Raberg, U. Ebels, S. O. Demokritov, J. Akerman *et al.*, Opportunities and challenges for spintronics in the microelectronics industry, *Nature Electronics* **3**, 446 (2020).
- [6] S. Datta and B. Das, Electronic analog of the electrooptic modulator, *Appl. Phys. Lett.* **56**, 665 (1990).
- [7] I. Žutić, J. Fabian, and S. D. Sarma, Spintronics: Fundamentals and applications, *Rev. Mod. Phys.* **76**, 323 (2004).
- [8] J. Schliemann, J. C. Egues, and D. Loss, Nonballistic Spin-Field-Effect Transistor, *Phys. Rev. Lett.* **90**, 146801 (2003).
- [9] X. Liu, X.-J. Liu, and J. Sinova, Spin dynamics in the strong spin-orbit coupling regime, *Phys. Rev. B* **84**, 035318 (2011).
- [10] H. C. Koo, J. H. Kwon, J. Eom, J. Chang, S. H. Han, and M. Johnson, Control of spin precession in a spin-injected field effect transistor, *Science* **325**, 1515 (2009).
- [11] J. Wunderlich, B.-G. Park, A. C. Irvine, L. P. Zârbo, E. Rozkotová, P. Nemeč, V. Novák, J. Sinova, and T. Jungwirth, Spin Hall effect transistor, *Science* **330**, 1801 (2010).
- [12] K. Olejník, J. Wunderlich, A. C. Irvine, R. P. Campion, V. P. Amin, J. Sinova, and T. Jungwirth, Detection of Electrically Modulated Inverse Spin Hall Effect in an Fe/GaAs Microdevice, *Phys. Rev. Lett.* **109**, 076601 (2012).
- [13] P. Chuang, S.-C. Hoo, L. W. Smith, F. Sfigakis, M. Pepper, C.-H. Chen, J.-C. Fan, J. P. Griffiths, I. Farrer, H. E. Beere, G. A. C. Jones, D. A. Ritchie, and T.-M. Chen, All-electric all-semiconductor spin field-effect transistors, *Nat. Nanotechnol.* **10**, 35 (2015).
- [14] W. Y. Choi, H.-J. Kim, J. Chang, S. H. Han, H. C. Koo, and M. Johnson, Electrical detection of coherent spin precession using the ballistic intrinsic spin Hall effect, *Nat. Nanotechnol.* **10**, 666 (2015).
- [15] W. Y. Choi, H.-J. Kim, J. Chang, S. H. Han, A. Abbout, H. B. M. Saidaoui, A. Manchon, K.-J. Lee, and H. C. Koo, Ferromagnet-free all-electric spin Hall transistors, *Nano Lett.* **18**, 7998 (2018).
- [16] W. Han, R. K. Kawakami, M. Gmitra, and J. Fabian, Graphene spintronics, *Nat. Nanotechnol.* **9**, 794 (2014).
- [17] J. H. Garcia, M. Vila, A. W. Cummings, and S. Roche, Spin transport in graphene/transition metal dichalcogenide heterostructures, *Chem. Soc. Rev.* **47**, 3359 (2018).
- [18] M. Gmitra, D. Kochan, P. Högl, and J. Fabian, Trivial and inverted Dirac bands and the emergence of quantum spin Hall states in graphene on transition-metal dichalcogenides, *Phys. Rev. B* **93**, 155104 (2016).
- [19] Z. Wang, D.-K. Ki, J. Y. Khoo, D. Mauro, H. Berger, L. S. Levitov, and A. F. Morpurgo, Origin and Magnitude

- of Designer' Spin-Orbit Interaction in Graphene on Semiconducting Transition Metal Dichalcogenides, *Phys. Rev. X* **6**, 041020 (2016).
- [20] B. Yang, M.-F. Tu, J. Kim, Y. Wu, H. Wang, J. Alicea, R. Wu, M. Bockrath, and J. Shi, Tunable spin-orbit coupling and symmetry-protected edge states in graphene/WS₂, *2D Mater.* **3**, 031012 (2016).
- [21] S. Zihlmann, A. W. Cummings, J. H. Garcia, M. Kedves, K. Watanabe, T. Taniguchi, C. Schönenberger, and P. Makk, Large spin relaxation anisotropy and valley-Zeeman spin-orbit coupling in WSe₂/graphene/*h*-BN heterostructures, *Phys. Rev. B* **97**, 075434 (2018).
- [22] T. Wakamura, F. Reale, P. Palczynski, S. Guéron, C. Mattevi, and H. Bouchiat, Strong Anisotropic Spin-Orbit Interaction Induced in Graphene by Monolayer WS₂, *Phys. Rev. Lett.* **120**, 106802 (2018).
- [23] A. W. Cummings, J. H. Garcia, J. Fabian, and S. Roche, Giant Spin Lifetime Anisotropy in Graphene Induced by Proximity Effects, *Phys. Rev. Lett.* **119**, 206601 (2017).
- [24] T. S. Ghiasi, J. Ingla-Aynés, A. A. Kaverzin, and B. J. van Wees, Large proximity-induced spin lifetime anisotropy in transition-metal dichalcogenide/graphene heterostructures, *Nano Lett.* **17**, 7528 (2017).
- [25] L. A. Benítez, J. F. Sierra, W. Savero Torres, A. Arrighi, F. Bonell, M. V. Costache, and S. O. Valenzuela, Strongly anisotropic spin relaxation in graphene-transition metal dichalcogenide heterostructures at room temperature, *Nat. Phys.* **14**, 303 (2018).
- [26] S. Omar, B. N. Madhushankar, and B. J. van Wees, Large spin-relaxation anisotropy in bilayer-graphene/WS₂ heterostructures, *Phys. Rev. B* **100**, 155415 (2019).
- [27] M. Offidani and A. Ferreira, Microscopic theory of spin relaxation anisotropy in graphene with proximity-induced spin-orbit coupling, *Phys. Rev. B* **98**, 245408 (2018).
- [28] M. Gmitra and J. Fabian, Proximity Effects in Bilayer Graphene on Monolayer WSe₂: Field-Effect Spin Valley Locking, Spin-Orbit Valve, and Spin Transistor, *Phys. Rev. Lett.* **119**, 146401 (2017).
- [29] J. Y. Khoo, A. F. Morpurgo, and L. Levitov, On-demand spin-orbit interaction from which-layer tunability in bilayer graphene, *Nano Lett.* **17**, 7003 (2017).
- [30] K. Zollner, M. Gmitra, and J. Fabian, Swapping Exchange and Spin-Orbit Coupling in 2D van der Waals Heterostructures, *Phys. Rev. Lett.* **125**, 196402 (2020).
- [31] Y. K. Luo, J. Xu, T. Zhu, G. Wu, E. J. McCormick, W. Zhan, M. R. Neupane, and R. K. Kawakami, Opto-valleytronic spin injection in monolayer MoS₂/few-layer graphene hybrid spin valves, *Nano Lett.* **17**, 3877 (2017).
- [32] A. Avsar, D. Unuchek, J. Liu, O. L. Sanchez, K. Watanabe, T. Taniguchi, B. Ozyilmaz, and A. Kis, Optospintronics in graphene via proximity coupling, *ACS Nano* **11**, 11678 (2017).
- [33] J. O. Island, X. Cui, C. Lewandowski, J. Y. Khoo, E. M. Spanton, H. Zhou, D. Rhodes, J. C. Hone, T. Taniguchi, K. Watanabe *et al.*, Spin-orbit-driven band inversion in bilayer graphene by the van der Waals proximity effect, *Nature (London)* **571**, 85 (2019).
- [34] C. K. Safeer, J. Ingla-Aynés, F. Herling, J. H. Garcia, M. Vila, N. Ontoso, M. R. Calvo, S. Roche, L. E. Hueso, and F. Casanova, Room-temperature spin Hall effect in graphene/MoS₂ van der Waals heterostructures, *Nano Lett.* **19**, 1074 (2019).
- [35] T. S. Ghiasi, A. A. Kaverzin, P. J. Blah, and B. J. van Wees, Charge-to-spin conversion by the Rashba-Edelstein effect in two-dimensional van der Waals heterostructures up to room temperature, *Nano Lett.* **19**, 5959 (2019).
- [36] L. A. Benítez, W. Savero Torres, J. F. Sierra, M. Timmermans, J. H. Garcia, S. Roche, M. V. Costache, and S. O. Valenzuela, Tunable room-temperature spin galvanic and spin Hall effects in van der Waals heterostructures, *Nat. Mater.* **19**, 170 (2020).
- [37] R. V. Gorbachev, F. V. Tikhonenko, A. S. Mayorov, D. W. Horsell, and A. K. Savchenko, Weak Localization in Bilayer Graphene, *Phys. Rev. Lett.* **98**, 176805 (2007).
- [38] S. Sugahara and J. Nitta, Spin-transistor electronics: An overview and outlook, *Proc. IEEE* **98**, 2124 (2010).
- [39] See Supplemental Material at <http://link.aps.org/supplemental/10.1103/PhysRevLett.127.047202> for sample fabrication, measurement details, additional measurements, and modeling details, which includes Refs. [40–55].
- [40] K. S. Novoselov, A. K. Geim, S. V. Morozov, D. Jiang, Y. Zhang, S. V. Dubonos, I. V. Grigorieva, and A. A. Firsov, Electric field effect in atomically thin carbon films, *Science* **306**, 666 (2004).
- [41] E. McCann and M. Koshino, The electronic properties of bilayer graphene, *Rep. Prog. Phys.* **76**, 056503 (2013).
- [42] A. Castellanos-Gomez, M. Buscema, R. Molenaar, V. Singh, L. Janssen, H. S. J. Van Der Zant, and G. A. Steele, Deterministic transfer of two-dimensional materials by all-dry viscoelastic stamping, *2D Mater.* **1**, 011002 (2014).
- [43] Y. Zhang, T.-T. Tang, C. Girit, Z. Hao, M. C. Martin, A. Zettl, M. F. Crommie, Y. R. Shen, and F. Wang, Direct observation of a widely tunable bandgap in bilayer graphene, *Nature (London)* **459**, 820 (2009).
- [44] D. A. Bandurin, I. Torre, R. Krishna Kumar, M. Ben Shalom, A. Tomadin, A. Principi, G. H. Auton, E. Khestanova, K. S. Novoselov, I. V. Grigorieva *et al.*, Negative local resistance caused by viscous electron backflow in graphene, *Science* **351**, 1055 (2016).
- [45] Y. Li and M. Koshino, Twist-angle dependence of the proximity spin-orbit coupling in graphene on transition-metal dichalcogenides, *Phys. Rev. B* **99**, 075438 (2019).
- [46] A. David, P. Rakyta, A. Kormányos, and G. Burkard, Induced spin-orbit coupling in twisted graphene-transition metal dichalcogenide heterobilayers: Twistronics meets spintronics, *Phys. Rev. B* **100**, 085412 (2019).
- [47] T. Maassen, I. J. Vera-Marun, M. H. D. Guimarães, and B. J. van Wees, Contact-induced spin relaxation in Hanle spin precession measurements, *Phys. Rev. B* **86**, 235408 (2012).
- [48] H. Idzuchi, A. Fert, and Y. Otani, Revisiting the measurement of the spin relaxation time in graphene-based devices, *Phys. Rev. B* **91**, 241407(R) (2015).
- [49] D. G. Purdie, N. M. Pugno, T. Taniguchi, K. Watanabe, A. C. Ferrari, and A. Lombardo, Cleaning interfaces in layered materials heterostructures, *Nat. Commun.* **9**, 5387 (2018).
- [50] F. Herling, C. K. Safeer, J. Ingla-Aynés, N. Ontoso, L. E. Hueso, and F. Casanova, Gate tunability of highly

- efficient spin-to-charge conversion by spin Hall effect in graphene proximitized with WSe₂, *APL Mater.* **8**, 071103 (2020).
- [51] J. C. Leutenantsmeyer, J. Ingla-Aynés, J. Fabian, and B. J. van Wees, Observation of Spin-Valley-Coupling-Induced Large Spin-Lifetime Anisotropy in Bilayer Graphene, *Phys. Rev. Lett.* **121**, 127702 (2018).
- [52] J. Xu, T. Zhu, Y. K. Luo, Y.-M. Lu, and R. K. Kawakami, Strong and Tunable Spin-Lifetime Anisotropy in Dual-Gated Bilayer Graphene, *Phys. Rev. Lett.* **121**, 127703 (2018).
- [53] Z. Yue, K. Tian, A. Tiwari, and M. E. Raikh, Spin transport in *n*-type single-layer transition-metal dichalcogenides, *Phys. Rev. B* **93**, 195301 (2016).
- [54] W. Han, J.-R. Chen, D. Wang, K. M. McCreary, H. Wen, A. G. Swartz, J. Shi, and R. K. Kawakami, Spin relaxation in single-layer graphene with tunable mobility, *Nano Lett.* **12**, 3443 (2012).
- [55] S. Kunschuh, M. Gmitra, D. Kochan, and J. Fabian, Theory of spin-orbit coupling in bilayer graphene, *Phys. Rev. B* **85**, 115423 (2012).
- [56] M. Venkata Kamalakar, A. Dankert, P. J. Kelly, and S. P. Dash, Inversion of spin signal and spin filtering in ferromagnet/hexagonal boron nitride-graphene van der Waals heterostructures, *Sci. Rep.* **6**, 21168 (2016).
- [57] J. Xu, S. Singh, J. Katoch, G. Wu, T. Zhu, I. Žutić, and R. K. Kawakami, Spin inversion in graphene spin valves by gate-tunable magnetic proximity effect at one-dimensional contacts, *Nat. Commun.* **9**, 2869 (2018).
- [58] T. Maassen, F. K. Dejene, M. H. D. Guimarães, C. Józsa, and B. J. van Wees, Comparison between charge and spin transport in few-layer graphene, *Phys. Rev. B* **83**, 115410 (2011).
- [59] W. Yan, O. Txoperena, R. Llopis, H. Dery, L. E. Hueso, and F. Casanova, A two-dimensional spin field-effect switch, *Nat. Commun.* **7**, 13372 (2016).
- [60] A. Dankert and S. P. Dash, Electrical gate control of spin current in van der Waals heterostructures at room temperature, *Nat. Commun.* **8**, 16093 (2017).
- [61] Z. G. Yu and M. E. Flatté, Spin diffusion and injection in semiconductor structures: Electric field effects, *Phys. Rev. B* **66**, 235302 (2002).
- [62] C. Józsa, M. Popinciuc, N. Tombros, H. T. Jonkman, and B. J. van Wees, Electronic Spin Drift in Graphene Field-Effect Transistors, *Phys. Rev. Lett.* **100**, 236603 (2008).
- [63] J. Ingla-Aynés, R. J. Meijerink, and B. J. van Wees, Eighty-eight percent directional guiding of spin currents with 90 μm relaxation length in bilayer graphene using carrier drift, *Nano Lett.* **16**, 4825 (2016).